LANGMUIR

Open Access
This article is licensed under CC-BY-NC-ND 4.0

pubs.acs.org/Langmuir Article

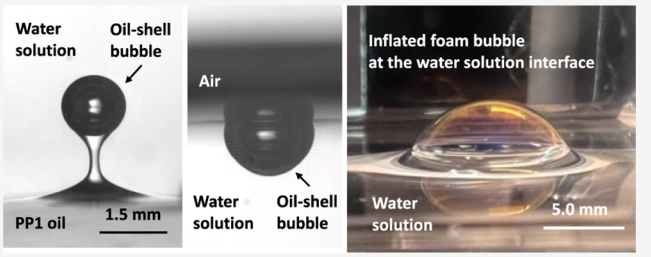
Self-Inflating Volatile Oil-Shell Bubbles and Foams Driven by Interfacial Air Diffusion

Ivan U. Vakarelski,* Farrukh Kamoliddinov, Sigurdur T. Thoroddsen, and Krassimir D. Danov

Cite This: *Langmuir* 2026, 42, 31793−31806 Read Online

ACCESS | Metrics & More | Article Recommendations | Supporting Information

ABSTRACT: Recent studies have shown that bubbles inside a volatile liquid can spontaneously grow in the absence of bulk gas supersaturation through diffusion of air driven by differences in its partial pressure. Here, we demonstrate a distinct manifestation of this phenomenon in which perfluorocarbon oil-shell bubbles, formed following bubble detachment from a perfluorocarbon oil (PP1, F2 Chemicals)−water interface, become trapped and spontaneously expand at the water−air interface. Addition of the anionic fluorosurfactant Capstone FS-60 to the aqueous phase stabilizes the detached oil-shell bubbles at the water−air interface. The bubbles spontaneously grow from an initial diameter of approximately 1.5 mm to several millimeters within a few minutes. The initial growth rate reaches about 11 μm/s, substantially exceeding that observed for bubbles trapped at the PP1−water interface. Bubble-bursting measurements indicate progressive thinning and eventual depletion of the PP1 shell at bubble radii of approximately 2.5−3.0 mm. Bubble growth nevertheless continues after shell depletion as the system transitions into a surfactant-stabilized foam bubble containing PP1 vapor. An interfacial air-diffusion model attributes the enhanced growth to the short diffusion path across the thin liquid film separating the bubble from the atmosphere, driven by the difference in air partial pressure between the PP1-vapor-containing bubble interior and the surrounding atmosphere. Finally, multiple oil-shell bubbles form self-expanding foam clusters that continue to grow for hours, increasing their apparent foam volume by more than 2 orders of magnitude. These findings demonstrate how modifying the mass-transfer geometry of interfacial air diffusion can strongly accelerate bubble growth and enable the formation of self-inflating bubbles and foams under ambient conditions.



INTRODUCTION

Gas bubble growth in liquids is commonly associated with a supersaturation-driven mass transfer and occurs in many natural and industrial systems.[1−4] Classical examples include carbonated beverages, boiling liquids, and gas evolution near heated surfaces.[5−11] In such systems, a bubble growth is typically driven by the diffusion of dissolved gas from a supersaturated liquid into the bubble interior and it is usually triggered by rapid external changes in pressure or temperature. Recently, we demonstrated a different type of spontaneous bubble growth in volatile liquids possessing both high vapor pressure and high gas solubility (perfluoro-2-methylpentane, C_6F_{14}, commercially available as PP1 from F2 Chemicals Ltd.), observed under ambient quiescent conditions.[12] In these systems, the bubble expansion can occur even in the absence of a bulk gas supersaturation, driven instead by the vapor-pressure-induced diffusion gradients between the bubble and the surrounding atmosphere. Similar types of spontaneous bubble expansion have also been reported in oil-recovery and oil-separation applications[13,14] and for volatile hydrocarbon vapor-containing self-expanding foams and bubbles.[15−17]

We demonstrated[12] self-inflating bubble growth within pure PP1 liquid under conditions of free evaporation from an open container. The spontaneous bubble growth is explained by the difference in PP1 vapor pressure inside the bubble and that above the freely evaporating PP1 interface. This pressure difference promotes diffusion of air into the bubble, leading to its growth. We also investigated bubble growth in PP1 when the liquid was in contact with a second air-saturated immiscible liquid placed above it: either ethanol, which has relatively high air solubility compared with water, or water, which has much lower air solubility than PP1. In both cases, the presence of the upper liquid phase accelerates bubble growth compared with bubbles in the bulk of freely evaporating PP1, indicating air mass transfer from the water or ethanol phase into the PP1 phase.

One of the experimental configurations used in our prior work involved bubbles trapped at the PP1−water or PP1−ethanol interface, as schematized in Figure 1a.[12] Figure 1b shows a snapshot example of such a bubble. In this

Received: June 23, 2026
Revised: October 8, 2026
Accepted: October 8, 2026
Published: October 19, 2026



ACS Publications
© 2026 The Authors. Published by American Chemical Society

https://doi.org/10.1021/acs.langmuir.6c03871
Langmuir 2026, 42, 31793−31806

Downloaded from pubs.acs.org/langd5/article-pdf/42/43/31793/6890141O/acs.langmuir.6c03871.pdf by guest on 08 November 2026

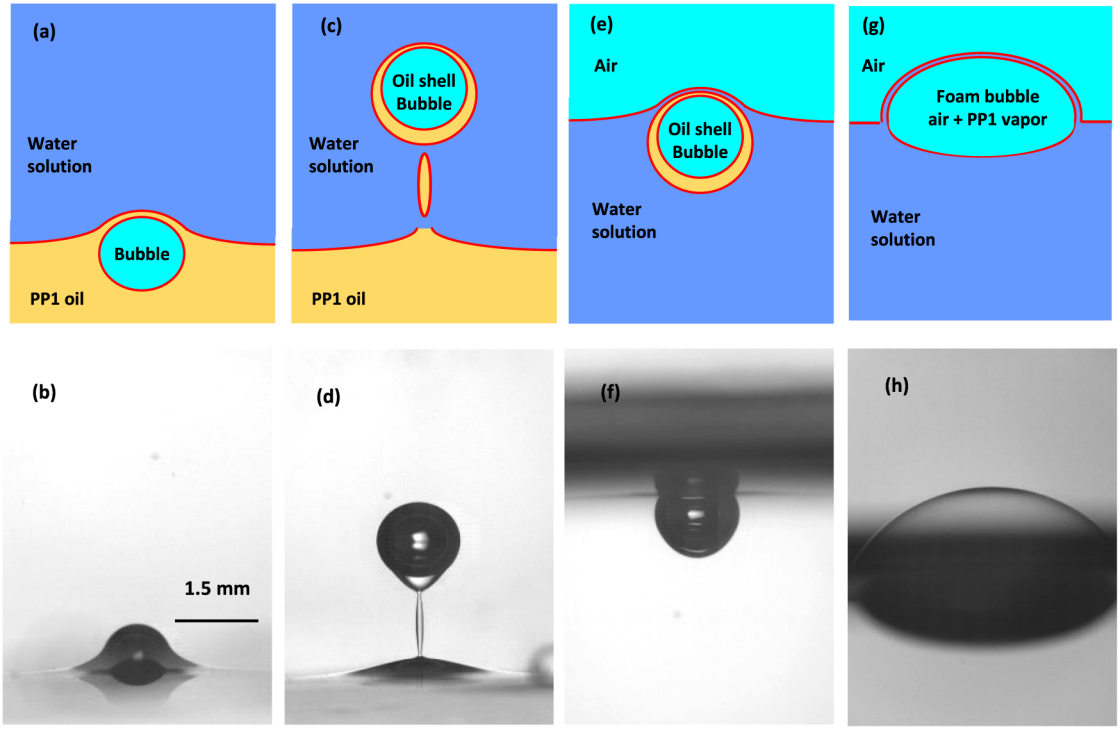


Figure 1. Schematics and high-speed camera snapshots illustrating: (a, b) a bubble trapped at the PP1−water interface; (c, d) an oil-shell bubble detaching from the PP1−water interface; (e, f) an oil-shell bubble trapped at the water solution−air interface; and (g, h) a foam bubble at the water solution−air interface following complete evaporation of the oil shell. In all cases, the bubble interior contains PP1 vapor. The high-speed video snapshots were obtained for the PP1−0.1 wt % FS-60 aqueous solution configuration.

configuration, the bubble is separated from the upper liquid phase by a thin PP1 film stabilized by the repulsive van der Waals forces in the air−PP1−water or air−PP1−ethanol systems.[18] As the bubble grows, it progressively deforms the PP1−water or PP1−ethanol interface. At a critical size (approximately 7.0 mm for PP1−pure water and 2.4 mm for PP1−ethanol), the buoyancy force can no longer be balanced by the capillary force associated with the curved interface, and the bubble detaches from the interface and enters the upper water or ethanol phase. Remarkably, as shown in Figure 1c schematics and illustrated by the snapshot in Figure 1d, the bubble entering the upper phase remains wrapped in a thin shell of fluorocarbon oil (PP1). The stability of this oil shell is attributed to the repulsive van der Waals forces typical for studied fluorocarbon oil systems.

Our previous investigation was limited to bubble inflation at the PP1−water or PP1−ethanol interface up to the moment of bubble detachment.[12] In the present study, we focus on the newly formed oil-shell bubbles when a surfactant is added to the aqueous phase, enabling stable bubble attachment to the water−air interface and its subsequent growth. Note that in pure water or ethanol, once a freely rising oil-shell bubble reaches the liquid−air interface, the thin liquid film formed upon collision ruptures rapidly, causing the bubble to coalesce with the atmosphere. Video 1 provides a real-time macroscopic visualization of this rapid collapse of an oil-shell bubble at the pure water−air interface. However, when an appropriate surfactant is added to the water phase, a stable foam film can form, trapping the bubble at the water−air interface. An additional benefit of the surfactant addition is the reduction of the water−PP1 interfacial tension, enabling control over the size of the detaching oil-shell bubbles.[19] A schematic of a bubble trapped at the surfactant solution−air interface is shown in Figure 1e, together with a representative snapshot of such a bubble in Figure 1f.

During the expansion of an oil-shell bubble at the surfactant solution−air interface, the oil shell can completely evaporate, transforming the oil-shell bubble into a foam bubble floating at the interface. Such bubbles still contain PP1 vapor in their interior, as schematically illustrated in Figure 1g and shown in the example image in Figure 1h.

In contrast to our previous bulk-liquid systems,[12] trapping the oil-shell bubbles at the solution−air interface reduces the diffusion path for atmospheric air into the bubble to only the thickness of the thin water/oil film at the bubble cap. Consequently, air diffusion through this thin film drives bubble expansion at rates approximately an order of magnitude faster than those observed in our previous study, ultimately enabling the spontaneous formation and growth of self-inflating foam clusters.

In recent studies, Kim and Ananth reported spontaneous foaming when a thin layer of a volatile hydrocarbon liquid is spread on an aqueous fluorosurfactant solution.[15,16] In their system, hydrocarbon vapor diffusion within the foam bubbles drives bubble growth but can also promote bubble rupture. Here, we demonstrate a different manifestation of this phenomenon, in which the expanding bubbles possess a volatile perfluorocarbon oil shell, giving rise to markedly different physicochemical behavior. Besides their high volatility and high air solubility, perfluorocarbons are chemically inert, and once the oil shell has completely evaporated, the perfluorocarbon vapor is not expected to significantly alter the water−air surface tension. Furthermore, unlike hydrocarbon-vapor foams, which are highly flammable, perfluor-

Downloaded from pubs.acs.org/langd5/article-pdf/42/43/31793/6890141O/acs.langmuir.6c03871.pdf by guest on 08 November 2026

https://doi.org/10.1021/acs.langmuir.6c03871
Langmuir 2026, 42, 31793−31806

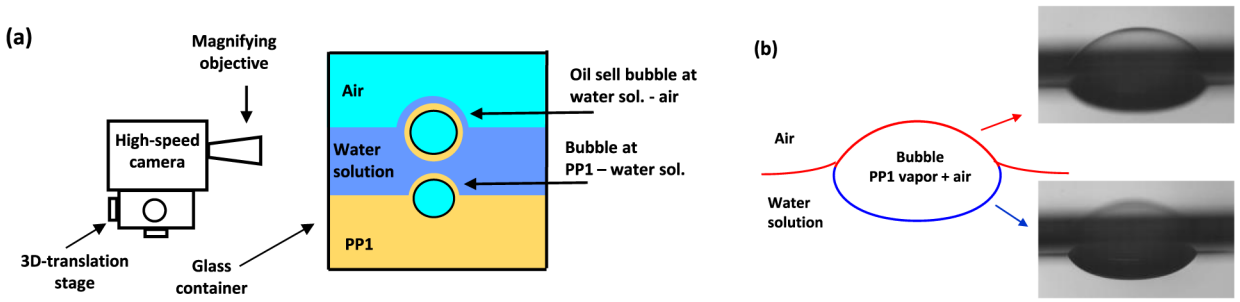


Figure 2. (a) Schematic of the experimental setup used for bubble observations. (b) Schematic of a bubble trapped at the air−water solution interface, consisting of an upper spherical-cap foam-film region (red) and a lower part immersed entirely in the aqueous phase (blue). The typical upper image is focused on the spherical-cap foam-film region, while the lower image is focused on the bottom part of the bubble.

ocarbon vapors are nonflammable, making such self-inflating bubbles and foam systems inherently safer.

Here, we present systematic observations and quantitative measurements of the spontaneous growth of PP1 oil-shell bubbles when an anionic fluorosurfactant, Capstone FS-60, is used to stabilize the thin liquid films formed upon the bubble attachment to the water−air interface. We identify distinct regimes of bubble growth and discuss the underlying physical mechanisms. Furthermore, we demonstrate that the oil-shell bubbles continue to grow after complete evaporation of the volatile PP1 shell, and that when multiple bubbles are released at the water−air interface, they spontaneously assemble into foam clusters that continue to expand for hours, resulting in an orders-of-magnitude increase in foam volume. These findings demonstrate that modifying the interfacial air diffusion geometry can considerably accelerate bubble growth, providing a simple strategy for engineering rapidly expanding bubbles and self-inflating foams.

MATERIALS AND EXPERIMENTAL METHODS

Materials

The perfluorocarbon liquid used in this study was FLUTEC PP1 (F2 Chemicals Ltd.), composed primarily of perfluoro-2-methylpentane (C_6F_{14}). The PP1 liquid density is 1.71 g/cm^3 and the dynamic viscosity is 0.78 mPa·s. The saturation vapor pressure of PP1 is 27 kPa and the vapor density is 0.013 g/mL. The surface tension of the liquid PP1-air interface was measured to be 12.4 mN/m. All cited properties correspond to atmospheric pressure and 25 °C, which is close to the laboratory temperature.

The water used was purified in a Millipore apparatus, with an internal specific electrical resistance of no less than 18.4 MΩ/cm. Ethanol of >99.7% absolute grade was purchased from Sigma-Aldrich. At room temperature and atmospheric pressure, the air solubility per 100 mL of liquid is highest in PP1 (44.2 mL of air volume), intermediate in ethanol (14.6 mL), and considerably lower in water (1.6 mL).[20]

The surfactant used was Capstone FS-60, a water-soluble anionic fluorosurfactant commonly employed as a high-performance wetting and leveling agent in aqueous formulations. Unless otherwise specified, experiments were performed at a surfactant concentration of 0.1 wt %. The static surface tension of the aqueous surfactant solutions, measured using the Wilhelmy plate method, was approximately 30.1 ± 0.5 mN/m at 0.001 wt % FS-60 and 17.2 ± 0.1 mN/m at 0.1 wt % FS-60. The static interfacial tension, σ, was measured at 25 °C by the Du Noüy ring method on force tensiometer K100 (Krüss, Germany) equipped with a platinum−iridium ring. The measured values were: σ = 51.2 ± 0.1 mN/m in the case of PP1−water interface; σ = 5.9 ± 0.1 mN/m for PP1−ethanol interface. The interfacial tension for PP1−FS-60 water solutions is measured by the drop shape analysis, and the interfacial tension is about 20 mN/m at 0.001 wt % FS-60. Above the critical micelle concentration, σ = 3.6 ± 0.1 mN/m for PP1−0.1 wt % FS-60 water solution.

Experimental Setups and Protocols

A general schematic of the experimental setup used to monitor bubble growth is shown in Figure 2a. Most experiments were conducted in an optical glass cell (Hellma Analytics) with a cross-section of 5.0 × 5.0 cm and a height of 5.0 cm, equipped with a glass cover lid. Prior to each experiment, the glass vessel was plasma cleaned and thoroughly rinsed with deionized water. The PP1 liquid was poured into the bottom of the cell to form a layer approximately 1 cm thick. On top of this layer, a 1−2 cm thick layer of water, ethanol, or, in most experiments, a FS-60 aqueous surfactant solution was carefully deposited. Following deposition of the upper liquid layer, a larger needle syringe was used to suck the interface and remove excess droplets and bubbles from both the PP1−water solution and water solution−air interfaces, thereby ensuring bubble clean interfaces prior to the experiments. During the experiments, the top of the container was kept closed in order to maintain saturation of water vapor in the air above the liquid.

Using a fine-needle syringe, a fresh millimeter-sized air bubble (≈0.5 to 1.0 mm) was released below the PP1−water solution interface. The bubble rose and became trapped at the PP1−water solution interface, as schematized in Figure 1a and illustrated in Figure 1b. Following detachment from the interface, the oil-shell bubble (Figure 1c,d) rose further and became trapped at the water surfactant solution−air interface (Figure 1e,f). The subsequent growth of the oil shell bubble and its transition into a foam bubble at the water solution−air interface (Figure 1g,h) was monitored and recorded.

The bubble detachment from the PP1−water solution interface and the subsequent growth of the oil shell bubbles at the top water solution−air interface was monitored and recorded using a high-speed camera (Photron SA5) equipped with a long-distance magnifying objective providing 1.5× magnification, resulting in an image resolution of approximately 19 μm/pixel. High-speed videos were typically recorded at 1000 frames per second (fps) for capturing the bubble detachment and free-rise processes, and at 60 fps for monitoring the longer-term growth of the oil-shell bubbles. The shutter speed was set to 1/5000 s in all experiments to minimize the motion blur and to improve the image sharpness and contrast.

In selected experiments, bubble growth at the water solution−air interface was also monitored using the optical imaging system and software of a DSA100E drop shape analyzer (Krüss, Germany), as employed in our previous study.[12] This system enabled long-term tracking of bubble growth with optical magnification, providing an image resolution of approximately 18 μm/pixel.

One experimental challenge in the monitoring bubble growth at the water solution−air interface was the high mobility of the bubbles and their tendency to migrate toward the cell walls. Whenever possible, the bubbles were tracked using the three-dimensional translation stage of the high-speed camera setup. As a result, some of the recorded videos may appear slightly jittery due to manual tracking adjustments.

Downloaded from pubs.acs.org/langd5/article-pdf/42/43/31793/6890141O/acs.langmuir.6c03871.pdf by guest on 08 November 2026

https://doi.org/10.1021/acs.langmuir.6c03871
Langmuir 2026, 42, 31793−31806

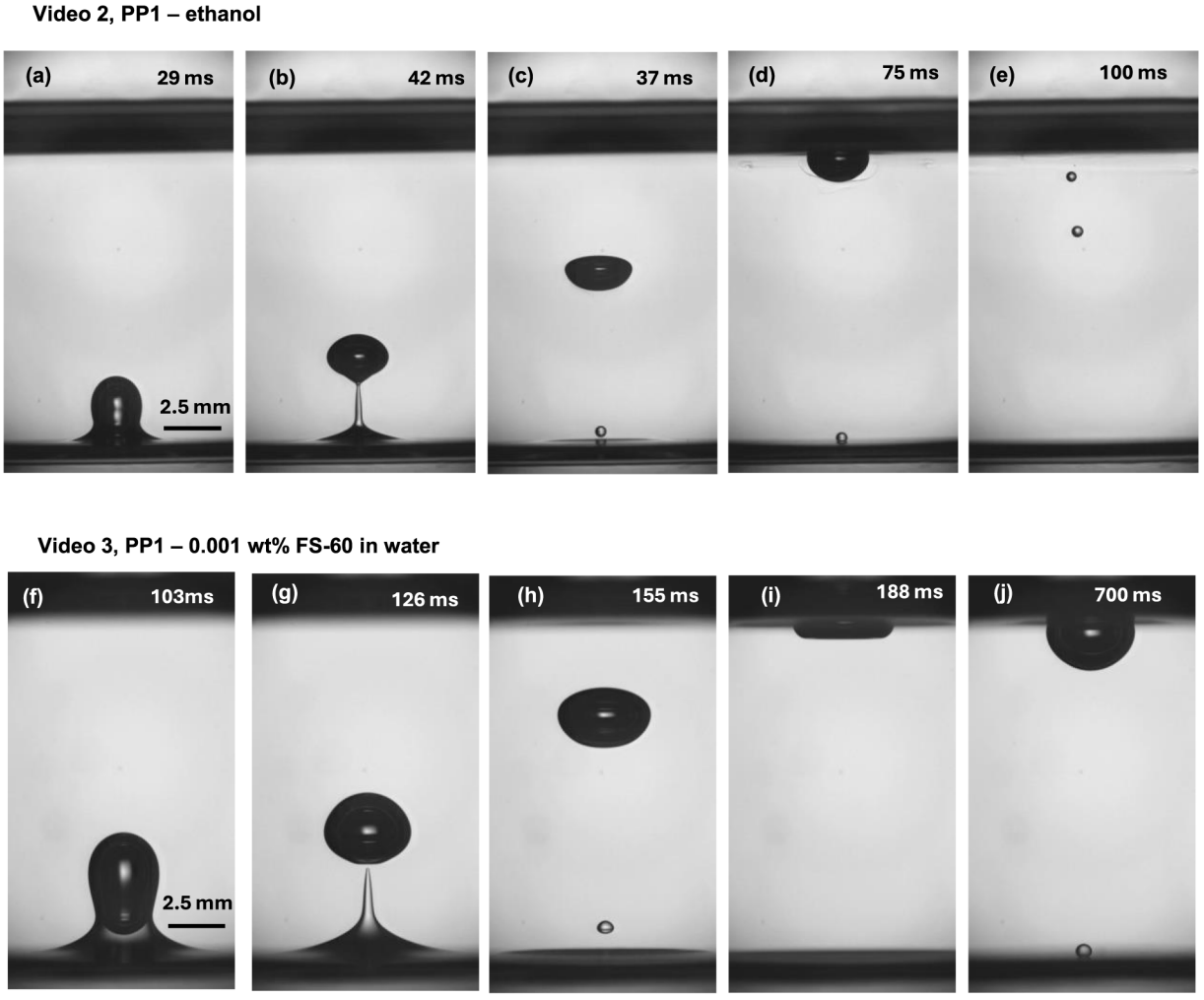


Figure 3. (a–e) Snapshots from Video 2 showing the evolution of a PP1 oil-shell bubble in the PP1–ethanol system: (a) just before detachment, (b) during detachment, (c) free rise, (d) collision with the ethanol–air interface, and (e) after coalescence, with two PP1 droplets falling downward. (f–g) Snapshots from Video 3 showing the evolution of a PP1 oil-shell bubble in the PP1–0.001 wt % FS-60 aqueous solution: (f) just before detachment, (g) during detachment, (h) free rise, (i) collision with the water–air interface, and (j) stabilization at the interface without coalescence.

The bubble growth was characterized in terms of the effective bubble radius, R, defined as the radius of a spherical bubble having the same volume as the observed bubble. As schematized in Figure 2b, bubbles trapped at the water solution–air interface consist of two parts: an upper spherical-cap region wrapped by a thin liquid film and a lower part immersed entirely in the aqueous phase. When only the upper part of the bubble is visible, the invisible lower part immersed in the aqueous phase is reconstructed numerically by solving the Young–Laplace equation. Conversely, when the lower part of the bubble is observed, the shape of the upper part is reconstructed by determining the best fit to the measured lower bubble profile. Details of the bubble at interface profile reconstruction and the volume determination can be found in our prior work.[12]

RESULTS AND DISCUSSION

Pure Water or Ethanol System vs Aqueous Surfactant Solution

Our primary focus in the present study is the expansion of surfactant-stabilized PP1 oil-shell bubbles trapped at the water–air interface. For comparison, we first briefly illustrate the behavior of oil-shell bubbles in the absence and presence of surfactant.

As established in our previous study, bubbles trapped at the PP1–water or PP1–ethanol interface spontaneously grow and eventually detach from the interface while remaining encapsulated by a thin PP1 oil shell.[12] The stability of this oil shell is associated with the repulsive van der Waals interaction characteristic of the air–PP1–water/ethanol systems.[15] In contrast, hydrocarbon oils generally have a higher refractive index than water (e.g., n = 1.43 for tetradecane), which leads to different interaction regimes.[18,21–25] Here, we focus on the subsequent behavior of these oil-shell bubbles after they rise through the upper liquid phase and reach the liquid–air interface.

Video 1 shows a macroscopic example for the PP1–pure-water system. Following detachment from the PP1–water interface, the oil-shell bubble rises through the water phase and rapidly coalesces upon reaching the water–air interface. Video 2 and Figure 3a–e show the corresponding process for the PP1–ethanol system. After detachment, the oil-shell bubble rises through the ethanol and rapidly coalesces at the ethanol–air interface, leaving small PP1 droplets that fall back into the liquid.

Downloaded from pubs.acs.org/langd5/article-pdf/42/43/31793/6890141O/acs.langmuir.6c03871.pdf by guest on 08 November 2026

https://doi.org/10.1021/acs.langmuir.6c03871
Langmuir 2026, 42, 31793–31806

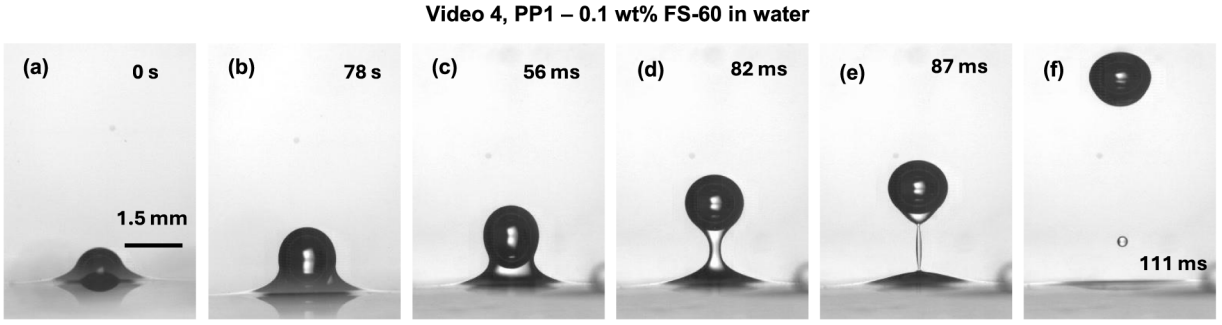


Figure 4. (a, b) Bubble at the PP1−0.1 wt % FS-60 water-solution interface shortly after becoming trapped at the oil−water interface (a) and just before detachment (b). (c−f) Snapshots from Video 4 showing details of bubble detachment from the interface (c−d) and subsequent free rise (f), recorded at a frame rate of 5000 fps.

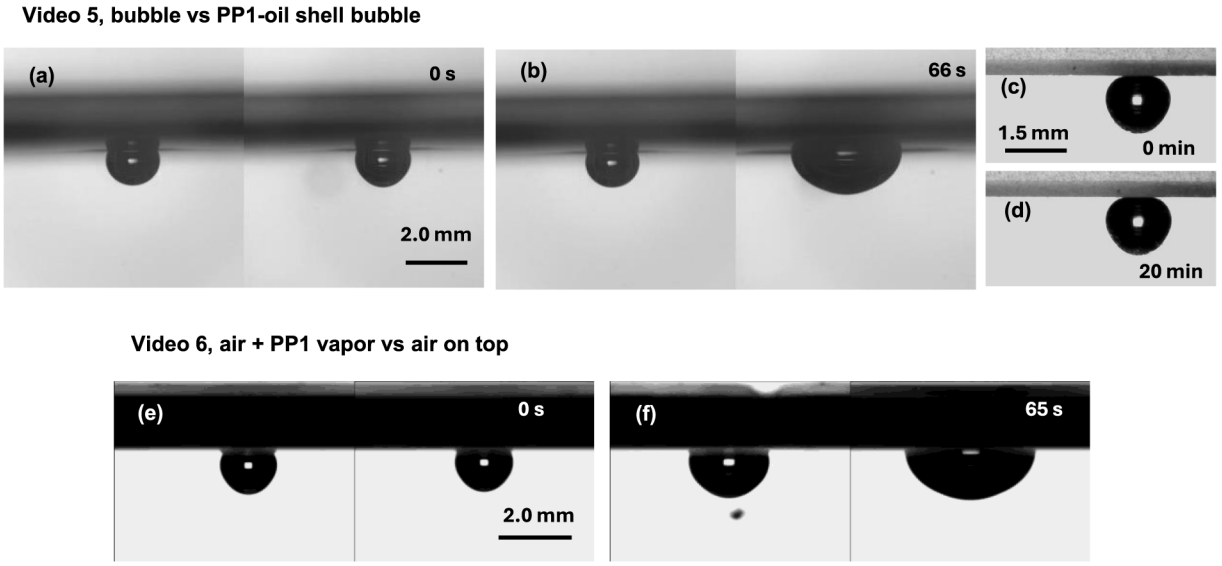


Figure 5. (a, b) Snapshots from Video 5 comparing a bubble without an oil shell trapped at the FS-60 aqueous solution−air interface (left) with an PP1 oil-shell bubble (right) after settling at the interface: (a) at the beginning of the recording and (b) approximately 66 s later. (c, d) PP1-oil shell bubble under a glass slide inside the water solution phase at the beginning of the recording and 20 min later showing no volume increase. (e, f) Snapshots from Video 6 comparing the growth of PP1 oil-shell bubbles in a PP1-vapor-enriched atmosphere (left) and in normal air (right): (e) at the beginning of the recording and (f) approximately 65 s later.

The rapid coalescence of the oil shell bubbles at the pure water−air or ethanol-air interface is expected, because for the PP1-water−air or PP1-ethanol-air film, the van der Waals force is now attractive and there are no other repulsive forces strong enough to stabilize the film, e.g., electric double layer repulsion. Additional factor for the fast coalescence of the bubble with the interfaces is the mobility of the pure water−air and ethanol−air interfaces[26] as well as hydrophobic attraction in the case of oil−water−air films.[27]

In contrast, addition of the anionic fluorosurfactant FS-60 to the aqueous phase prevents immediate coalescence and allows the oil-shell bubble to remain trapped at the water−air interface. Video 3 and Figure 3f−j illustrates this behavior for a low FS-60 concentration of 0.001 wt %. At this concentration, the reduced PP1−water interfacial tension results in detachment at a smaller bubble radius, approximately R = 1.75 mm compared to R = 3.50 mm in pure water. Following detachment and free rise through the aqueous phase, the oil-shell bubble becomes temporarily stabilized at the water−air interface rather than immediately coalescing.

The stability of the air−PP1−water−air film in the presence of surfactant is attributed to adsorption of the anionic surfactant at both water−air and PP1−water interfaces, resulting in reduced interfacial tensions and electric double layer repulsive stabilization of the film. In the example shown in Video 3, the low surfactant FS-60 concentration of 0.001 wt % allows the bubbles to remain trapped at the interface for up to 60 s before collapsing. Increasing the concentration to 0.1 wt % of FS-60 provides longer-term stabilization of the film and enables systematic investigation of the self-inflation of bubbles trapped at the water−air interface.

Oil-Shell Bubbles at the Water Solution (0.1 wt % FS-60)−Air Interface

In this set of experiments, we investigate the inflation of oil-shell bubbles after they become trapped at the water−air interface. To enable systematic measurements, the surfactant concentration (FS-60) is fixed at 0.1 wt %. At this surfactant concentration, corresponding to interfacial tension of 3.6 ± 0.1 mN/m, the initial radius of the oil-shell bubbles is approximately R = 0.75 ± 0.5 mm.

Video 4 shows the formation and detachment of an oil-shell bubble from the PP1−0.1 wt % FS-60 solution interface. Videos 5−8 then examine the subsequent bubble growth under

Downloaded from pubs.acs.org/langd5/article-pdf/42/43/31793/6890141410/acs.langmuir.6c03871.pdf by guest on 08 November 2026

https://doi.org/10.1021/acs.langmuir.6c03871
Langmuir 2026, 42, 31793−31806

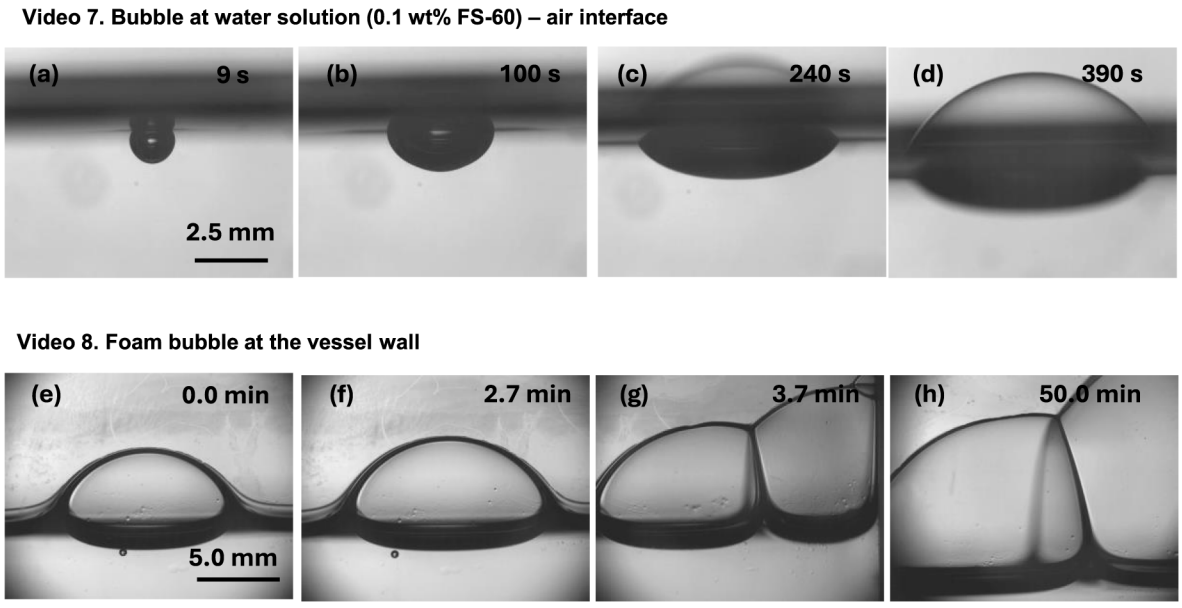


Figure 6. (a–d) Time-sequence snapshots from Video 7 showing the growth of a PP1 oil-shell bubble at the 0.1 wt % FS-60 water solution–air interface. (e–h) Time-sequence snapshots from Video 8 showing the growth of wall-attached foam bubble. Note that the focal plane in Video 8 is at the vessel wall, showing the foam bubble meniscus in contact with the wall rather than the thin liquid film (bubble cap) separating the floating bubble from the atmosphere. In each snapshot from Video 7a–d and Video 8e–h, the corresponding real time from the video beginning is indicated.

different configurations: comparison with an ordinary air bubble (Video 5), the effect of PP1-vapor-enriched air (Video 6), extended growth at the water solution–air interface (Video 7), and long-term growth after attachment to the vessel wall (Video 8).

Before detachment, the bubble grows at the PP1–0.1 wt % FS-60 solution interface at approximately $J_R = dR/dt = 2.4 \pm 0.2$ μm/s (Figure 4a,b). This value is close to the characteristic growth rate previously measured for bubbles at the PP1–pure water interface, $J_R = 1.7$ μm/s.[12] The interfacial air diffusion mechanism responsible for the bubble growth at the PP1–water interface was discussed in detail in our previous investigation.[12] Video 4 and Figure 4c–f show the subsequent bubble detachment and formation of the freely rising oil-shell bubble. During detachment, the bubble pinches off a thin PP1 thread and rapidly relaxes to a stable shape. A slight downward deformation remains at the bottom of the rising bubble, indicating a thicker oil layer in this region.

Video 5 provides a proof-of-concept demonstration comparing an ordinary air bubble released into the aqueous surfactant solution without the PP1 layer and subsequently trapped at the water–air interface compared to an oil-shell bubble trapped under the same conditions. Figure 5 shows snapshots from this video at the beginning (Figure 5a) and toward the end of the recording (Figure 5b). The video clearly shows that, whereas the ordinary bubble exhibits no measurable growth, the oil-shell bubble undergoes a significant expansion over the real-time duration of the recording (66 s) from R = 0.75 mm to R = 1.6 mm. This observation confirms that the bubble growth is driven by the presence of the oil shell.

In another experiment, a horizontal glass slide was placed inside the aqueous solution phase. After detachment from the interface, the oil-shell bubble became trapped beneath the glass slide, as shown in the snapshot in Figure 5c. Figure 5d shows the same bubble 20 min later. No measurable bubble growth was observed during this period. This result indicates that, for bubbles trapped at the water–air interface, air diffusion toward the bubble occurs through the thin liquid film separating the upper part of the bubble from the air phase above it.

To further verify that the driving force for bubble expansion is the difference in air partial pressure between the bubble interior and the atmosphere above the bubble, we performed a control experiment in which a small vial containing PP1 was placed above the aqueous solution inside the closed observation cell. Evaporation of PP1 from the vial increased the PP1 vapor concentration in the air above the bubble, thereby reducing the air partial-pressure difference driving air diffusion into the bubble.

Video 6 compares the growth of oil-shell bubbles in the presence of PP1-vapor-enriched air (left) and in normal air (right). Figure 5e and f show snapshots from the beginning and the end of the recording, respectively. The video clearly demonstrates that the presence of PP1 vapor above the bubble strongly suppresses bubble growth. In the PP1-vapor-enriched atmosphere, the bubble radius increased only from R = 0.8 mm to R = 1.1 mm, whereas in normal air the same bubble expanded from R = 0.8 mm to R = 1.7 mm over the same period. It should be noted that the air above the bubble was not expected to become fully saturated with PP1 vapor because the observation cell could not be completely sealed. The top cover had to be opened repeatedly during the experiment to introduce fresh bubbles into the PP1 phase, allowing some exchange with the ambient air. Consequently, bubble growth was significantly reduced but not completely suppressed, as would be expected under fully PP1-vapor-saturated conditions. This experiment provides strong support for the proposed interfacial air diffusion mechanism, in which the air partial-pressure difference across the thin liquid film is the driving force for spontaneous bubble inflation.

Video 7 tracks the growth of a bubble at the interface over an extended period of 420 s. As mentioned in the Experimental

https://doi.org/10.1021/acs.langmuir.6c03871
Langmuir 2026, 42, 31793–31806

Downloaded from pubs.acs.org/langd5/article-pdf/42/43/31793/6890141O/acs.langmuir.6c03871.pdf by guest on 08 November 2026

section, one of the main challenges in tracking bubble growth over long times is the high transverse mobility of bubbles at the water−air interface and their tendency to migrate toward the cell walls. Consequently, Video 7 provides the longest continuous observation of bubble growth obtained before the bubble migrated to the wall of the observation cell.

Figure 6a−d presents time-lapse snapshots extracted from Video 7, illustrating the bubble growth process. As the bubble expands, it progressively emerges above the interface driven by the buoyancy, and by the end of the recording a spherical foam-bubble dome is clearly formed (Figure 6d). Figure 7a tracks the effective bubble radius as a function of time, extracted from Video 7. The initial bubble radius is approximately R = 0.75 mm, increasing to about R = 3.6 mm by the end of the recording.

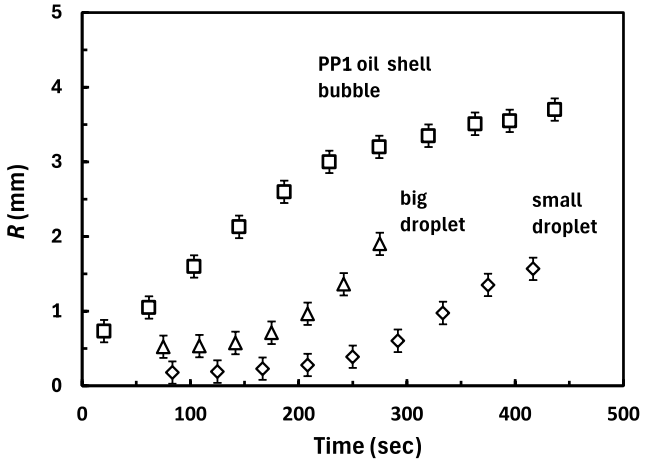


Figure 7. Effective bubble radius, *R*, as a function of time, *t*, for bubbles at the 0.1 wt % FS-60 water solution−air interface: oil-shell bubble data extracted from Video 7 (squares), and bubbles inside small (diamonds) and large (triangles) emulsion droplets, both extracted from Video 9. Error bars represent the uncertainty in the determination of the effective bubble radius. The reproducibility of the oil-shell bubble growth measurements is demonstrated by multiple independent experiments, shown in Supplementary Figure S1.

The graph in Figure 7 reveals two distinct regimes of bubble growth. In the initial, steeper regime, corresponding to growth from R = 0.75 mm to R = 3.0 mm (from 0 to 300 s), the measured radial growth rate is approximately $J_R \approx 11.1 \pm 0.4$ μm/s. This rate significantly exceeds the growth rate observed for bubbles at the PP1−water solution interface (approximately 2.4 μm/s). Subsequently, the bubble growth rate decreases to approximately $J_R \approx 3.0 \pm 0.3$ μm/s. The reproducibility of the oil-shell bubble growth measurements is demonstrated in Supplementary Figure S1, which compares the results from three independent experiments.

As was seen toward the end of Video 7, the soap bubbles tend to migrate toward the vessel walls. The bubbles then become attached to the vessel wall without bursting. Once attached to the wall, the bubbles are observed to continue expanding over extended periods of time (hours). An example of this behavior is shown in Video 8, where a wall-attached bubble continues to grow with snapshots from this video presented in Figure 6e−h. Eventually, the bubble slips along the wall and attaches to another bubble located in the corner of the cell (Figure 6g). The final part of the video, captured after a time lapse of approximately 50 min, demonstrates the continued expansion of the wall-attached bubbles (Figure 6h). The initial bubble size is R = 0.75 mm while the final bubble size observed in Video 8 reached about 1.5 cm in length, corresponding to an increase in bubble volume of approximately 2 orders of magnitude. Clusters of such bubbles form a foam layer, which is discussed in the "Self-expanding foam" section.

Bubble in Emulsion Droplet

An alternative approach to studying the oil-shell bubble expansion at the interface is to use bubbles seeded within emulsion droplets. As in our prior study, bubbles are seeded in the emulsion droplet during the droplet impact on the water interface.[12] This bubble is caught at the center of the droplet impact.[28] In the present experiment, the bubble seeded emulsion droplets are deposited onto the PP1−water solution

Video 9. Small and large bubble in emulsion droplet expansion

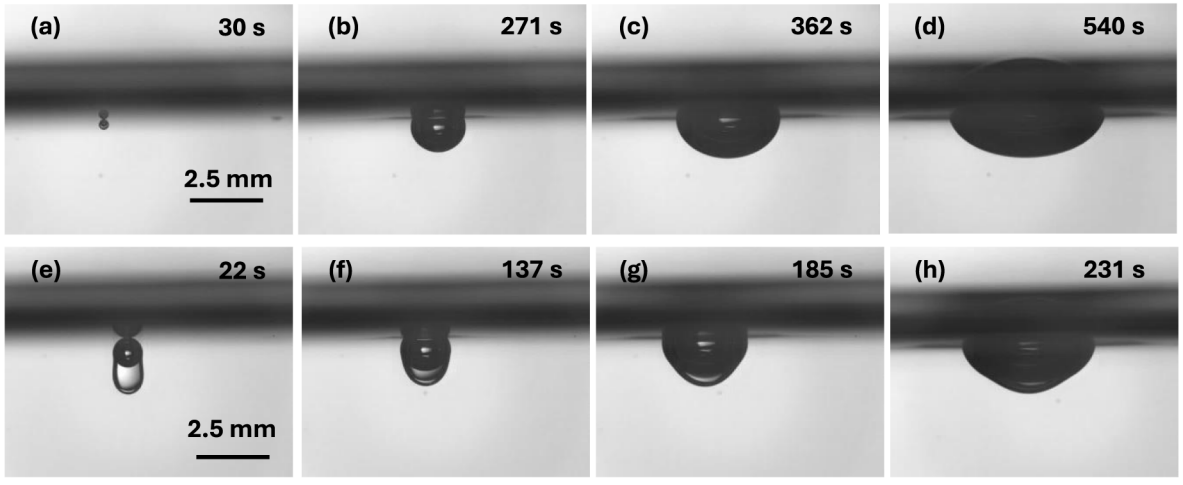


Figure 8. (a−d) Time-sequence snapshots from composite Video 9 showing the growth of bubble inside small emulsion droplets (a−d) and large emulsion droplets (e−h). In each snapshot from Video 9, the corresponding real time from the video beginning is indicated. The snapshot in (d) is taken after a time lap of about 177 s from the end of the video.

Downloaded from pubs.acs.org/langd5/article-pdf/42/43/31793/6890141O/acs.langmuir.6c03871.pdf by guest on 08 November 2026

https://doi.org/10.1021/acs.langmuir.6c03871
Langmuir 2026, 42, 31793−31806

interface. Due to the presence of surfactants, the droplet does not coalesce with the interface. As the encapsulated bubbles gradually inflate, the droplets become buoyant and rise, eventually settling at the water−air interface.

Video 9 compares the evolution of a bubble within small and large emulsion droplet. The initial bubble diameters are approximately 0.25 mm and 1.2 mm, respectively. In both cases, the bubble in emulsion droplet at water solution−air interfaces expansion proceeds in a manner similar to that observed for oil-shell bubbles. Figure 8a−d present a time-sequence of snapshots for the bubble in the smaller emulsion droplet, while Figure 8e−h shows the corresponding sequence for the larger emulsion droplet.

Figure 7 presents the time dependence of bubble effective radius for the small and large emulsion droplets in comparison to the oil-shell bubble. In both cases, the initial growth rate is slower than that observed for oil-shell bubbles formed by the transition through PP1-water solution interface. This is attributed to the fact that, at early stages, the bubbles inside emulsion droplets configurations are less buoyant as a whole than the oil-shell bubbles resulting in comparably smaller thin film areas facing the air. However, the growth rate of the larger bubble eventually accelerates and reaches values close to those measured for the oil-shell bubbles at the top interface.

Remarkably, even the bubble in the small emulsion droplet exhibits accelerated growth over time, ultimately reaching a final diameter of approximately 5.0 mm, corresponding to an increase in volume of more than 3 orders of magnitude (Figure 8d). In the case of the smaller droplet, it is evident that the oil phase evaporates completely at an early stage of the growth process. In contrast, for the larger droplet, the oil phase remains clearly visible at the lower part of the bubble until the end of the recording. In the next section, we quantify the evaporation of the oil shell.

Oil Shell Evaporation

The bubble growth is driven by both air diffusion through the thin liquid film and evaporation of PP1 vapor into the bubble. The PP1 saturation vapor pressure is about 27 kPa or about 27% than that of the atmospheric pressure, P_{atm} = 100 kPa. Over time, PP1 evaporation progressively depletes the oil shell, which may eventually disappear completely. One way to monitor the progression of oil-shell evaporation is to observe the oil droplets left behind following bubble bursting.

Occasionally, the bubbles burst at different stages of their growth, most likely due to contamination at the interface. In such cases, a small oil droplet (or two) is observed to fall downward, which is presumed to originate from the bubble's oil shell. As the bubble size increases, the remaining droplet size decreases, consistent with the progressive evaporation and depletion of the oil shell during bubble growth. Remarkably, above a critical bubble size (approximately R = 3.0 mm), no droplet emission is observed, indicating that the oil shell has been completely depleted. Video 10 illustrates this effect by comparing the bursting of a smaller bubble (left side, R = 1.1 mm) with that of a much larger bubble (right, R = 3.5 mm). Figure 9 presents snapshots from this video, showing the bubbles immediately before and after bursting for the smaller bubble (Figure 9a,b) and the larger bubble (Figure 9c,d). Small PP1 oil droplets are clearly observed falling dawn after the bursting of the smaller bubble, whereas no such droplets are observed following the bursting of the larger bubble.

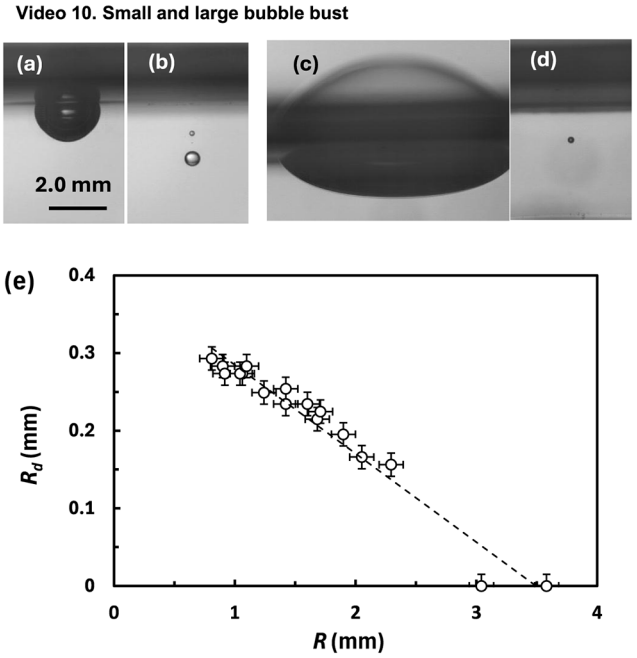


Figure 9. (a−d) Snapshots from Video 10 showing the bubbles immediately before and after bursting for the smaller bubble, R = 1.1 mm (a, b) and the larger bubble, R = 3.5 mm (c, d). Two PP1 droplets are observed falling after the bursting of the smaller bubble, whereas no droplets are observed following the bursting of the larger bubble (the small black dot is a bubble which rises up). (e) Dependence of the falling droplets effective radius, R_d, on the busted bubble radius, R. The straight line represents an empirical linear fit to the data. The error bars reflect the precision with which the droplets and bubbles radius is determined.

Figure 9e shows the dependence of the effective radius of the falling PP1 droplets, R_d, on the effective bubble radius at the moment of bursting, R, obtained from multiple experiments. The trend of decreasing droplet size with increasing bubble size is clearly evident. The straight line represents an empirical linear fit to the data and predicts complete evaporation of the oil shell at a bubble radius of approximately R = 3.5 mm, in good agreement with the experimental observations. This result is also consistent with the decrease in bubble growth rate observed once the bubble radius exceeds R = 3.0 mm in Figure 7.

From the measured droplet sizes, it is possible to estimate the bubble volume at which the oil shell completely evaporates under the assumption that the bubble interior remains fully saturated with PP1 vapor. Taking the largest measured PP1 droplet, corresponding to the bursting of the smallest bubble (R_d = 0.3 mm, R = 0.8 mm), we estimate that the oil shell becomes fully depleted at a bubble size of approximately, R = 2.5 mm. Similar results were obtained using other droplet/bubble sizes, e.g., R = 2.5 ± 0.2 mm. Considering the approximate nature of this analysis and the dynamic character of the bubble growth process, these values are in good agreement with the experimental observation that no oil droplets are emitted when bubbles larger than approximately R = 3.0 mm burst. Together, these results place the radius at which the oil shell is fully depleted in the range of approximately R = 2.5−3.0 mm. Future studies using more advanced experimental techniques, such as fluorescence labeling or refractive-index imaging, could provide a more precise determination of the oil-shell depletion point.

Downloaded from pubs.acs.org/langd5/article-pdf/42/43/31793/6890141410/acs.langmuir.6c03871.pdf by guest on 08 November 2026

https://doi.org/10.1021/acs.langmuir.6c03871
Langmuir 2026, 42, 31793−31806

In conclusion, our results indicate that for bubble sizes exceedingly R = 2.5 to 3.0 mm, the oil shell has completely evaporated. Nevertheless, the bubbles continue to grow even after the shell has fully evaporated, ablate at a slower rate. At this stage, the system transitions from an oil-shell bubble to a conventional surfactant-stabilized foam bubble at the water−air interface, distinguished by the presence of PP1 vapor within the bubble interior.

Interfacial Air Diffusion Mechanism for Oil-Shell and Foam Bubbles at Water Solution Interface

The bubble growth in multicomponent liquid systems has been widely studied for solutions containing nonvolatile solutes[29,30] as well as volatile liquid mixtures.[31−34] Here, we discuss the interfacial air diffusion mechanism in the case of volatile oil-shell bubbles trapped at the water solution−air interface and the subsequent formation of floating foam bubbles containing volatile oil vapor (PP1 vapor in the present study).

A simplified schematic of an oil-shell bubble sitting under the water solution−air interface is shown in Figure 10. The bubble is characterized by an effective radius, R, and a two-layer thin liquid film hemispherical cap with a total thickness $h = h_w + h_p$, where h_w and h_p are the thicknesses of the aqueous and PP1 layers, respectively. As experimentally demonstrated (Figure 5), air diffusion toward the bubble occurs exclusively through bubble cap thin liquid film area.

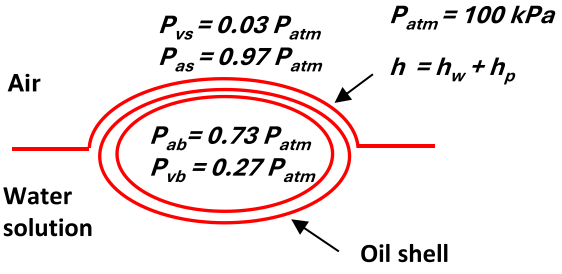


Figure 10. Simplified schematic of a PP1 oil-shell bubble at the water solution−air interface with indicated partial air and vapor pressures inside and outside the bubble. The bubble is characterized by an effective radius, R, and an upper thin liquid film of total thickness, $h = h_w + h_p$, where h_w and h_p are the thicknesses of the aqueous and PP1 layers, respectively. The partial pressure of air inside the bubble is approximately $p_{ab} \approx 73$ kPa, whereas the partial pressure of air above the bubble is approximately $p_{sb} \approx 97$ kPa. This creates a partial air-pressure difference of $\Delta p_a \approx 24$ kPa, which drives air diffusion through the thin liquid-film cap and the associated bubble expansion.

The diffusion coefficient of the PP1 vapor molecules in air, D_{vb}, is equal to 6×10^{-6} m^2/s. For a bubble of radius R = 0.75 mm the corresponding characteristic diffusion time, R^2/D_{vb}, is approximately 0.09 s. This is more than 2 orders of magnitude shorter than the characteristic bubble-growth time (tens of seconds to minutes). Therefore, as long as the oil shell has not completely evaporated, vapor diffusion within the bubble is sufficiently rapid to maintain the PP1 partial pressure close to its saturation value, justifying the assumption of vapor−liquid equilibrium used in the model.

In conventional foams, bubble growth or shrinkage is typically governed by Laplace-pressure differences between neighboring bubbles, which drive gas diffusion from smaller, high-pressure bubbles to larger, low-pressure bubbles.[35−38] However, for the parameters of the present system, the Laplace capillary pressure, p_c inside the bubble can be estimated to be negligible compared to the atmospheric and PP1 vapor pressure. Using characteristic values for the water solution surface tension, $\sigma = 18$ mN/m, and the bubble radii, $R > 0.75$ mm, in our experiments, we estimate that $p_c = 2\sigma/R < 0.05$ kPa. This is negligible compared to the atmospheric pressure, $P_{atm} \approx 100$ kPa, and the PP1 saturated vapor pressure of about 27 kPa. Therefore, under the ambient quiescent conditions of the experiments, the total pressure inside the bubble can be approximated as equal to the atmospheric pressure:

$$P_{atm} = p_{vb} + p_{ab} = p_{vs} + p_{as} \tag{1}$$

Here, p_{vb} and p_{ab} are the partial pressures of PP1 vapor and air inside the bubble, respectively. Under present experimental conditions, the air above the aqueous surface is assumed to be fully saturated with water vapor. We also assume that the PP1 vapor diffusivity through the water film to be negligible. Thus, p_{vs} and p_{as} denote the partial pressures of water vapor and air above the solution surface. Assuming full saturation of the bubble interior with PP1 vapor, $p_{vb} \approx 27$ kPa, giving $p_{ab} \approx 73$ kPa. Above the water, $p_{vs} \approx 3$ kPa and therefor $p_{as} \approx 97$ kPa. This results in a characteristic air partial-pressure difference:

$$\Delta p_a = p_{as} - p_{ab} \approx 0.24 P_{atm} = 24\ \text{kPa} \tag{2}$$

This substantial partial-pressure difference drives continuous diffusion of air through the thin liquid film into the bubble, resulting in spontaneous bubble inflation.

For foam films, the molar air flux per unit bubble area, J_a, can be described by the solution−diffusion model:

$$J_a = P_h(\Delta p_a / h) \tag{3}$$

where P_h is the air permeability coefficient of the liquid film and h is the foam-film thickness. The permeability coefficient is given by $P_h = DS$, where D is the diffusion coefficient of air in the liquid film and S is the solubility of air in the liquid. This formulation is commonly used to describe gas transport through foam films.[35,36]

In our case, the film consists of two layers, $h = h_w + h_p$ where h_w water-layer thickness and h_p the PP1-layer thickness. Because the air solubility in the PP1 film is much higher than in water, approximately 27 times higher,[20] while the air diffusion coefficient is similar in both liquids, the permeability coefficient of water is much smaller than that of PP1. Furthermore, the PP1 film thickness in the bubble cap region is governed by the short-ranged repulsive van der Waals forces and is expected to be comparatively smaller than the water-film thickness, which is stabilized by the longer ranged repulsive electric double-layer forces. Therefore, as a good approximation, the overall mass-transfer resistance is controlled primarily by the aqueous layer, and eq 3 is evaluated using the water effective permeability coefficient and $h \approx h_w$.

When considering the diffusivity and solubility of air in water, we keep in mind that the air is a gas mixture comprised primary of nitrogen ($N_2 \approx 78\%$) and oxygen ($O_2 \approx 21\%$). Accordingly, weighted-average values are used in the model. The effective diffusion coefficient of air in water is taken as, $D \approx 2 \times 10^{-9}$ m^2/s, while the effective molar solubility of air in water is approximated as, $S \approx 1 \times 10^{-5}$ mol m^{-3} Pa^{-1}. Using the relation $P_h = DS$ the corresponding air permeability coefficient is estimated as, $P_h \approx 2 \times 10^{-14}$ mol m^{-1} s^{-1} Pa^{-1}, which is used in the present model. We also note that higher surfactant concentrations can increase the air solubility, S, through micellar solubilization,[39] and recent measurements of thick fluorosurfactant films have demonstrated strongly

Downloaded from pubs.acs.org/langd5/article-pdf/42/43/31793/6890141410/acs.langmuir.6c03871.pdf by guest on 08 November 2026

https://doi.org/10.1021/acs.langmuir.6c03871
Langmuir 2026, 42, 31793−31806

Video 11. Bubble cluster formation

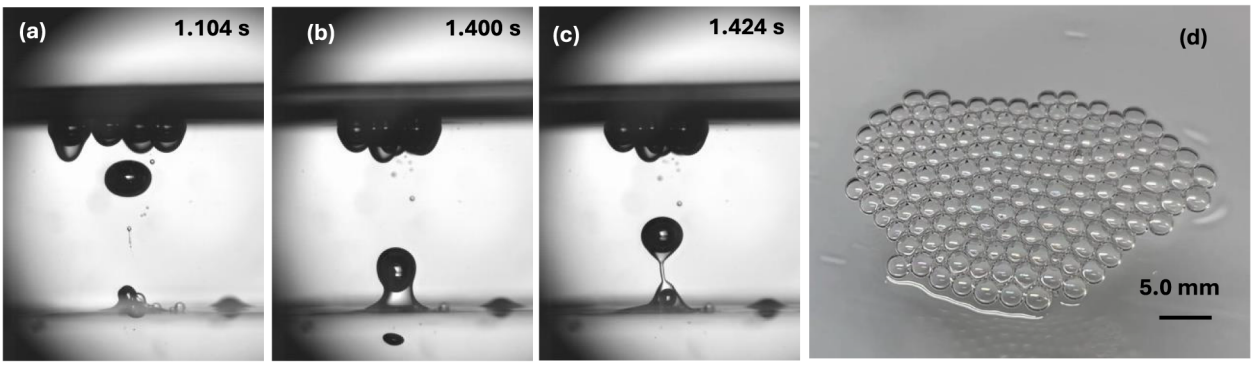


Figure 11. (a–c) Snapshots from Video 11 illustrating the formation of a bubble cluster by continuous injection of small bubbles below the PP1–water solution interface. The injected bubbles coalesce beneath the interface before detaching as larger oil-shell bubbles. (d) Phone-camera image of an oil-shell bubble cluster accumulated at the water solution–air interface following continuous bubble injection.

enhanced permeability above a critical permeability concentration several times the critical micelle concentration (CMC).[40] However, at the relatively low surfactant concentration used here (0.1 wt %, approximately twice the CMC), the effect of micellar solubilization on air transport is expected to be small.

From the mass balance describing bubble growth, the bubble radius growth rate is given by

$$dR/dt = (R_g T/p_{ab})J_a \tag{4}$$

where R_g = 8.314 J mol^{-1} K^{-1} is the universal gas constant, and T = 298 K is the room temperature. Combining eqs 3 and 4 yields

$$dR/dt = (R_g T P_h \Delta p_a)/(p_{ab} h) \tag{5}$$

This relation connects the experimentally observed bubble growth rate with the relevant physical properties of the system, namely the gas permeability coefficient, the partial pressure difference across the film, bubble internal air pressure, and foam-film thickness.

To check the consistency of the model, eq 5 can be rearranged to estimate the unknown film thickness, h, using the experimentally measured bubble growth rate:

$$h = (R_g T P_h \Delta p_a)/(p_{ab}(dR/dt)) \tag{6}$$

From the experimental data shown in Figure 7 extracted from Video 7, the effective bubble-radius growth rate is approximately $dR/dt \approx 11$ μm/s for bubble size between R = 1.0 to 2.5 mm, during the stage in which the oil shell has not yet evaporated. However, because gas diffusion occurs only through the foam-film cap region of the bubble, and because approximately half of the bubble surface is submerged in this size range, the local growth rate associated with diffusion through the active foam-film area should be taken to be about twice the apparent effective growth rate. Therefore, in the estimate using eq 6, we use $dR/dt \approx 22$ μm/s as the effective local bubble growth rate through the foam-film cap.

Substituting the parameters into eq 6, namely $R_g T P_h \approx 4.95 \times 10^{-11}$ m s^{-1}, $\Delta p_a \approx 24$ kPa, $p_{ab} \approx 73$ kPa, and $dR/dt \approx 2.2 \times 10^{-5}$ m s^{-1}, gives $h \approx 0.7$ μm. An average foam-cap water-film thickness of less than one micron is reasonable for a large aqueous film stabilized by repulsive electric double-layer forces. At the same time, we recognize that this represents only an average value over the spatial and temporal evolution of the film during bubble expansion. Thus, this estimate supports the overall consistency of the proposed model rather than providing independent validation. A more quantitative validation could be achieved in future work by directly measuring the thin liquid-film thickness using interferometry, as previously demonstrated for bubbles approaching a flat glass surface.[41] Such measurements, combined with the measured bubble growth rate, could also provide an independent estimate of the effective liquid-film permeability, P_h.

It is important to note that, prior to evaporation of the oil shell, bubble growth results from the simultaneous mass transfer of air into the bubble and evaporation of PP1 into the expanding bubble volume in order to maintain PP1 vapor saturation. Equation 4 represents the mass balance of air in the bubble. Under the condition that the vapor inside the bubble remains saturated with PP1 vapor, the corresponding mass balance for PP1 gives $dR/dt = (R_g T/p_{av})J_v$, where J_v is the PP1 vapor molar flux per unit bubble area. Equating the two expressions for dR/dt yields $J_v/J_a = p_{vb}/p_{ab} = (0.27P_{atm})/(0.73P_{atm}) \approx 0.37$.

Next, we consider bubble expansion after the oil shell has completely evaporated and the bubble has transitioned from an oil-shell bubble to a foam bubble containing PP1 vapor. After complete evaporation of the PP1 oil shell at an effective bubble radius, R_p, experimentally $R_p \approx 2.5$ mm, the number of PP1 vapor moles inside the bubble becomes fixed. Consequently, the PP1 vapor partial pressure decreases as the bubble volume increases according to, $p_{vb} = 0.27P_{atm}(R_p/R)$.[3] Assuming that the total pressure inside the bubble remains approximately atmospheric, P_{atm}, then, $p_{ab} = P_{atm} - p_{vb}$, and the driving pressure difference for air diffusion becomes approximately $\Delta p_a \approx p_{vb}$. Substituting these expressions into eq 5 gives

$$dR/dt = (R_g T P_h/h)((0.27(R_p/R)^3/(1 - 0.27(R_p/R)^3)) \tag{7}$$

For, $R > R_p$, the denominator varies comparatively weakly, and therefore the bubble growth rate can be approximated as

$$dR/dt \sim R^{-3} (for\ R > R_p) \tag{8}$$

indicating that the bubble expansion rate decreases rapidly with increasing bubble size after complete evaporation of the oil shell.

https://doi.org/10.1021/acs.langmuir.6c03871
Langmuir 2026, 42, 31793–31806

Downloaded from pubs.acs.org/langd5/article-pdf/42/43/31793/6890141O/acs.langmuir.6c03871.pdf by guest on 08 November 2026

Video 12. Expending foam bubble cluster

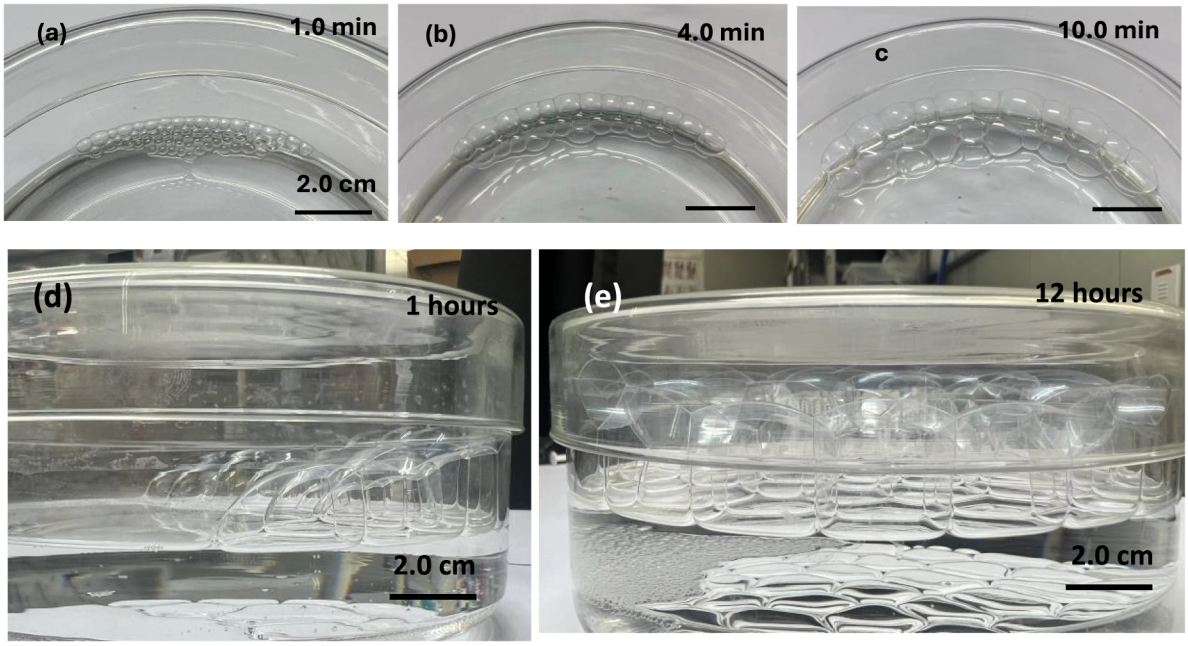


Figure 12. (a–c) Snapshots from Video 12 showing the expansion of a foam-bubble cluster approximately 1 min (a), 4 min (b), and 10 min (c) after the cluster became attached to the vessel wall. (d, e) Side-view images of representative foam-bubble clusters after approximately 1 h (d) and 12 h (e) of expansion. The images illustrate the continued growth and coarsening of the foam long after the initial formation of the bubble cluster.

Taking the experimental value R_p = 2.5 mm, bubble radius of R = 3.5 mm corresponds to R/R_P = 1.4. According to eq 7, this gives $dR/dt \approx 0.30\ (dR/dt)_{Rp}$. This estimate is in reasonable agreement with the experimental data in Figure 7, extracted from Video 7, where dR/dt decrease from approximately 11 μm/s at R = 2.5 mm, to approximately 3 μm/s at R = 3.5 mm. This agreement further supports the consistency of the proposed physical picture.

We expect the general trend predicted by eq 8, namely that the bubble growth rate scales approximately as, $dR/dt \sim R^{-3}$ to also hold for bubbles within a foam-bubble cluster. However, the situation in clustered foams is considerably more complex because of the heterogeneous foam structure and the coupled gas transfer between neighboring bubbles. A more complete description would therefore require the development of a more sophisticated model together with dedicated experiments.

Expanding Foam Bubble Clusters

Finally, we demonstrate the potential of oil-shell bubbles to form self-expanding foams. The experiments are conducted in a crystallizer dish with a diameter of 14 cm and a depth of 7 cm. As in the single-bubble experiments, a ∼1 cm thick layer of PP1 is placed at the bottom of the dish, and ∼2 cm of the aqueous solution is carefully added on top.

To rapidly generate multiple bubbles, air was continuously injected into the PP1 phase using the fine needle syringe. The oil-shell bubbles forming in that way are illustrated in Video 11, with representative snapshots shown in Figure 11a–c. During this bubble generation, multiple smaller bubbles coalesce beneath the PP1–water solution interface until a sufficiently large bubble detaches. Due to the dynamic nature of the process, the bubbles produced in this manner are generally larger (about 2 mm in diameter) than the spontaneously detaching bubbles described earlier. They also carry a larger oil cap beneath them, similar to the behavior observed for bubbles originating in emulsion droplets. Although bubble production by continuous injection is less well controlled than the spontaneous detachment mechanism at the PP1–water solution interface, it enables rapid generation of large clusters of relatively monodisperse bubbles, such as the cluster shown in Figure 11d.

An important precondition for foam bubbles long-term stability is that the vessel lid is closed shortly after bubble deposition, to maintain high water-vapor saturation in the air above the foam. We also observe that a single bubble floating at the interface is less stable than a cluster of bubbles. Furthermore, clusters that accumulate at the vessel wall exhibit enhanced long-term stability.

Figure 12a shows a snapshot of a bubble cluster at the vessel wall shortly after formation. Video 12 is a composite time-lapse recording that follows the subsequent self-expansion of this cluster. The video shows the bubble cluster at 3 min (Figure 12a), 6 min (Figures 12b) and 10 min (Figure 12c) after formation, clearly demonstrating continuous growth. Figure 12d is a side view image of a similar bubble cluster after 60 min. Although some foam films collapse over time, the remaining bubbles continue to expand, resulting in an overall increase in the foam volume by more than 2 orders of magnitude within 60 min. At the beginning of the video, the bubble size within the cluster is approximately 3 mm, increasing to about 2 cm by the end of the recording.

A further example is shown in Figure 12e, where another batch of bubbles was left overnight. The side-view image shows the formation of coarse foam with bubbles of approximately 3 cm in size, filling the entire volume of the vessel. As noted above, the oily shell has completely evaporated at a much earlier stage. These observations demonstrate that even low concentrations of PP1 vapor are sufficient to sustain the diffusion mechanism over extended periods. It also indicates

Downloaded from pubs.acs.org/langd5/article-pdf/42/43/31793/6890141O/acs.langmuir.6c03871.pdf by guest on 08 November 2026

https://doi.org/10.1021/acs.langmuir.6c03871
Langmuir 2026, 42, 31793–31806

that the foam films are significantly more permeable to air molecules than to PP1 vapor molecules.

The foam expansion results presented herein are included primarily to demonstrate the capability of this approach to create self-expanding foams. Future work will focus on quantifying the process, optimizing the volatile oil−surfactant system, improving long-term foam stability, and exploring potential practical applications of these self-expanding bubble and foam systems.

CONCLUSIONS

In this work, we investigated the spontaneous growth of perfluorocarbon oil-shell bubbles formed after the bubble detachments from a PP1−aqueous surfactant solution interface and subsequent trapping at the water−air interface. The addition of the anionic fluorosurfactant FS-60 stabilized the thin liquid film separating the bubble from the atmosphere, enabling long-term observation of the bubble growth. The oil-shell bubbles exhibited spontaneous inflation, increasing from submillimeter dimensions to several millimeters within a few minutes. The initial growth rate of approximately 11 μm/s was substantially higher than that observed for bubbles trapped at the PP1−water interface. Comparison with ordinary air bubbles and with oil-shell bubbles trapped in the bulk aqueous phase confirmed that the growth originates from the volatile PP1 shell and is driven by air diffusion through the thin liquid film covering the bubble. Furthermore, control experiments performed in a PP1-vapor-enriched atmosphere confirmed that the bubble growth is governed by the difference in air partial pressure between the bubble interior and the atmosphere above the bubble.

Analysis of the bubble bursting events and the size of the falling oil droplets showed that the oil shell progressively evaporates during bubble growth and becomes completely depleted when the bubble radius reaches approximately 2.5−3.0 mm. Despite the disappearance of the oil shell, the bubble growth continues. At this stage, the system transitions into a surfactant-stabilized soap bubble at the water−air interface containing PP1 vapor in its interior. To explain this behavior, we extended the interfacial air diffusion model developed in our previous work.[12] The model shows that the difference in the air partial pressure between the PP1-vapor-saturated bubble interior and the humid atmosphere above the aqueous phase generates a driving force for continuous air diffusion into the bubble. The resulting partial-pressure difference of approximately 24 kPa provides a strong driving force for the spontaneous bubble inflation.

Finally, we demonstrated that multiple oil-shell bubbles can form self-expanding foam clusters. The foam continued to grow for hours, increasing its volume by more than 2 orders of magnitude even after complete evaporation of the oil shells. Unlike conventional foam coarsening, which is driven by Laplace-pressure differences between neighboring bubbles, the growth observed here is driven by vapor-pressure-induced air diffusion from the atmosphere into the bubbles.

These results reveal a new route for generating self-inflating bubbles and foams under ambient conditions and provide new insight into mass-transfer-driven bubble dynamics in volatile liquids with high vapor pressure and high gas solubility. More broadly, the ability of trace amounts of volatile vapor to sustain long-term bubble and foam expansion under ambient conditions may open new opportunities for the development of self-inflating soft materials and related functional systems.

ASSOCIATED CONTENT

Supporting Information

The Supporting Information is available free of charge at https://pubs.acs.org/doi/10.1021/acs.langmuir.6c03871.

Figure S1: reproducibility of oil-shell bubble growth (PDF)

Video 1: phone-camera video showing the detachment of an oil-shell bubble from the PP1−pure water interface and its rapid coalescence at the water−air interface, real-time duration: 4.1 s (MP4)

Video 2: high-speed video showing the detachment of an oil-shell bubble from the PP1−ethanol interface, its free rise, and subsequent coalescence at the ethanol−air interface, real-time duration: 0.678 s (MP4)

Video 3: high-speed video showing the detachment of an oil-shell bubble from the PP1−0.001 wt % FS-60 aqueous solution interface, its free rise, and subsequent stabilization at the water solution−air interface, real-time duration: 0.701 s (MP4)

Video 4: high-speed video showing in detail the detachment of an oil-shell bubble from the PP1−0.1 wt % FS-60 aqueous solution interface and its subsequent free rise, real-time duration: 0.134 s (MP4)

Video 5: side-by-side comparison of an ordinary air bubble without an oil shell (left) and a PP1 oil-shell bubble (right) trapped at the FS-60 0.1 wt % aqueous solution−air interface, real-time duration: 66.7 s (MP4)

Video 6: side-by-side comparison of a oil-shell bubble trapped at the FS-60 0.1 wt % aqueous solution−air interface in the case of a PP1-vapor-enriched atmosphere (left) and in normal air (right), real-time duration: 65.0 s (MP4)

Video 7: the growth of a PP1 oil-shell bubble at the FS-60 0.1 wt % aqueous solution−air interface, real-time duration: 450 s (MP4)

Video 8: the growth of a foam bubble attached to the vessel wall, real-time duration: 303 s (MP4)

Video 9: the growth of bubbles inside a small (left) and a large (right) emulsion droplet at the FS-60 0.1 wt % aqueous solution−air interface, real-time duration: 363 s (MP4)

Video 10: the bursting of a smaller bubble (R = 1.1 mm, left) and a larger bubble (R = 3.5 mm, right) at the FS-60 0.1 wt % aqueous solution−air interface, real-time duration: 2.5 s (MP4)

Video 11: the formation of a PP1 oil-shell bubble cluster at the FS-60 0.1 wt % aqueous solution−air interface by continuous injection of small bubbles below the PP1−water solution interface, real-time duration: 2.0 s (MP4)

Video 12: phone-camera time-lapse video showing the expansion of a foam-bubble cluster approximately 1 min (0−6 s), 4 min (6−10 s), and 10 min (10−14.5 s) after the cluster became attached to the vessel wall (MP4)

AUTHOR INFORMATION

Corresponding Author

Ivan U. Vakarelski − *Division of Physical Sciences and Engineering, King Abdullah University of Science and Technology (KAUS), Thuwal 23955-6900, Saudi Arabia; Department of Chemical and Pharmaceutical Engineering, Faculty of Chemistry and Pharmacy and Center of*

Downloaded from pubs.acs.org/langd5/article-pdf/42/43/31793/6890141O/acs.langmuir.6c03871.pdf by guest on 08 November 2026

Competence "Smart Mechatronic, Eco- and Energy-Saving Systems, and Technologies", Sofia University, Sofia 1164, Bulgaria; orcid.org/0000-0001-9244-9160;
Email: ivakarelski@gmail.com

Authors

Farrukh Kamoliddinov − *Division of Physical Sciences and Engineering, King Abdullah University of Science and Technology (KAUS), Thuwal 23955-6900, Saudi Arabia;* orcid.org/0000-0001-5582-9893

Sigurdur T. Thoroddsen − *Division of Physical Sciences and Engineering, King Abdullah University of Science and Technology (KAUS), Thuwal 23955-6900, Saudi Arabia;* orcid.org/0000-0001-6997-4311

Krassimir D. Danov − *Department of Chemical and Pharmaceutical Engineering, Faculty of Chemistry and Pharmacy and Center of Competence "Smart Mechatronic, Eco- and Energy-Saving Systems, and Technologies", Sofia University, Sofia 1164, Bulgaria*

Complete contact information is available at: https://pubs.acs.org/10.1021/acs.langmuir.6c03871

Notes

The authors declare no competing financial interest.

■ ACKNOWLEDGMENTS

The work was supported by the King Abdullah University of Science and Technology (KAUST) under baseline grants BAS/1/1352-01-01. The authors acknowledge the financial support of Project CoC "Smart Mechatronics, Eco- and Energy-Saving Systems and Technologies", No. BG16RFPR002-1.014-0005, funded by the European Regional Development Fund under the Operational Program "Scientific Research, Innovation and Digitization for Smart Transformation 2021−2027." The authors gratefully acknowledge Dr. Rumyana D. Stanimirova for performing the surface and interfacial tension measurements.

■ REFERENCES

(1) Epstein, P. S.; Plesset, M. S. On the stability of gas bubbles in liquid-gas solutions. *J. Chem. Phys.* **1950**, *18*, 1505−1509.
(2) Scriven, L. E. On the dynamics of phase growth. *Chem. Eng. Sci.* **1959**, *10*, 1−13.
(3) Bankoff, S. G. Diffusion-controlled bubble growth. In *Advances in Chemical Engineering*; Academic Press, 1966. Vol. *6*, pp 1−60, .
(4) Plesset, M. S.; Prosperetti, A. Bubble dynamics and cavitation. *Annu. Rev. Fluid. Mech.* **1977**, *9*, 145−185.
(5) Jones, S. F.; Evans, G. M.; Galvin, K. P. Bubble nucleation from gas cavities − a review. *Adv. Colloid Interface Sci.* **1999**, *80*, 27−50.
(6) Bisperink, C. G. J.; Prins, A. Bubble growth in carbonated liquids. *Colloids Surf., A* **1994**, *85*, 237−253.
(7) Liger-Belair, G. The physics behind the fizz in champagne and sparkling wines. *Euro. Phys. J. Spec. Top.* **2012**, *201*, 1−88.
(8) Vignes-Adler, M. The fizzling foam of champagne. *Angew. Chem., Int. Ed.* **2013**, *52*, 187−190.
(9) Prosperetti, A.; Plesset, M. S. Vapor-bubble growth in a superheated liquid. *J. Fluid Mech.* **1978**, *85*, 349−368.
(10) Kolev, N. I. Bubble growth in superheated liquid. In *Multiphase Flow Dynamics*; Springer: Berlin, Heidelberg, 2011; pp. 35−66.
(11) Vakarelski, I. U.; Chan, D. Y. C.; Marston, J. O.; Thoroddsen, S. T. Dynamic air layer on textured superhydrophobic surfaces. *Langmuir* **2013**, *29*, 11074−11081.
(12) Vakarelski, I. U.; Marinova, K.; Danov, K. D.; D, K. Spontaneous bubble growth inside high-saturation-vapor-pressure and high-air-solubility liquids and emulsion droplets. *Langmuir* **2025**, *41*, 2071−2081.
(13) Kim, D. H.; Jung, M. C.; Cho, S.-H.; Kim, S. H.; Kim, H.-Y.; Lee, H. J.; Oh, K. H.; Moon, M.-W. UV-responsive nano-sponge for oil absorption and desorption. *Sci. Rep.* **2015**, *5*, 12908.
(14) Kim, M.-S.; Ko, T.-J.; Kim, J. S.; Lee, Y.-.; Oh, A. K. H.; Moon, M.-W. Multiple air-bubble enhanced oil rupture on nanostructured cellulose fabric for easy-oil cleaning fouled in a dry state. *Sci. Rep.* **2019**, *9*, 14538.
(15) Kim, K. D.; Ananth, R. Spontaneous aqueous foaming with fluorosurfactants from a hydrocarbon liquid at ambient conditions. *Colloids Surf., A* **2023**, *663*, 131048.
(16) Kim, K. D.; Ananth, R. Anomalous diffusion of hydrocarbon vapor through an aqueous foam bubble structure. *Colloids Surf., A* **2024**, *702*, 134937.
(17) Kim, D. K.; Ananth, R. An air-breathing hydrocarbon-vapor bubble from a surfactant film *Colloids Surf*. *Colloids Surf., A* **2026**, *728*, 138548.
(18) Li, E. Q.; Vakarelski, I. U.; Chan, D. Y. C.; Thoroddsen, S. T. Stabilization of thin liquid films by repulsive van der Waals force. *Langmuir* **2014**, *30*, 5162−5169.
(19) Herchenbach, P. J.; Layman, B. R.; Dick, J. E. Quantifying the interfacial tension of adsorbed droplets on electrified interface. *J. Colloid Interface Sci.* **2024**, *674*, 474−481.
(20) *F2 Chemicals Ltd.* https://f2chemicals.com (Accessed 2026−06−08).
(21) Li, E. Q.; Al-Otaibi, S.; Vakarelski, I. U.; Thoroddsen, S. T. Satellite formation during bubble transition through an interface between immiscible liquids. *J. Fluid Mech* **2014**, *744*, R1.
(22) Farhadi, J.; Sattari, A.; Hanafizadeh, P. Passage of a rising bubble through a liquid-liquid interface: A flow map for different regimes. *Can. J. Chem. Eng.* **2021**, *100*, 221−436.
(23) Shen, M.; Li, B.Q. Bubble rising and interaction in ternary fluid flow: a phase field study. *RSC Adv.* **2023**, *13*, 3561−3574.
(24) Li, Y.; Jiang, B.; Xiao, X.; Yang, N.; Sun, Y.; Zhang, L. Bubble Behavior and Surface Liquid Film Characteristics of Air Bubbles Crossing the Oil−Water Interface. *Symmetry* **2024**, *16*, 1564.
(25) Liu, D.; Cheng, Y.; Xiao, B.; Jiang, C. Droplet encapsulating bubble: Investigation of droplet spreading dynamics and bubble encapsulation time. *Phys. Fluids* **2026**, *38*, 012129.
(26) Vakarelski, I. U.; Yang, F.; Thoroddsen, S. T. Free-rising bubbles bounce more strongly from mobile than from immobile water-air interfaces. *Langmuir* **2020**, *36*, 5908−5918.
(27) Vakarelski, I. U.; Kamoliddinov, F.; Thoroddsen, S. T. Why bubbles coalesce faster than droplets: The effects of interface mobility and surface charge. *Langmuir* **2024**, *40*, 11340−1135.
(28) Thoraval, M.-J.; Thoroddsen, S. T. Contraction of an air disk caught between two different liquids. *Phys. Rev. E* **2013**, *88*, 061001.
(29) Miyatake, O.; Tanaka, I.; Lior, N. A simple universal equation for bubble growth in pure liquids and binary solutions with a non-volatile solute. *Int. J. Heat Mass Transfer.* **1997**, *40*, 1577−1584.
(30) Dias, J. P.; Barbosa, J. R., Jr.; Prata, A. T. Dynamics of gas bubble growth in oil-refrigerant mixtures under isothermal depressurization. *J. Braz. Soc. Mech. Sci. Eng.* **2012**, *34*, 155−166.
(31) Bertoldi, D.; Dallalba, C. C. S.; Barbosa, J. R., Jr. Experimental investigation of two-phase flashing flows of a binary mixture of infinite relative volatility in a Venturi tube. *Exp. Therm. Fluid Sci.* **2015**, *64*, 152−163.
(32) Suhas, B. G.; Sathyabhama, A. Bubble dynamics of water-ethanol mixture during subcooled flow boiling in a conventional channel. *Appl. Therm. Eng.* **2017**, *113*, 1596−1609.
(33) Cai, C.; Liu, H.; Xi, X.; Jia, M.; Yin, H. Bubble growth model in uniformly superheated binary liquid mixture. *Int. J. Heat Mass Transfer.* **2018**, *127*, 629−638.
(34) Ozturk, T.; Erbil, H. Y. Simple model for diffusion-limited drop evaporation of binary liquids from physical properties of the components: Ethanol−water example. *Langmuir* **2020**, *36*, 1357−1371.

Downloaded from pubs.acs.org/langd5/article-pdf/42/43/31793/6890141O/acs.langmuir.6c03871.pdf by guest on 08 November 2026

(35) Farajzadeh, R.; Krastev, R.; Zitha, P. L. J. Foam Film Permeability: Theory and Experiment. *Adv. Colloid Interface Sci.* **2008**, *137*, 27−44.
(36) Farajzadeh, R.; Muruganathan, R. M.; Rossen, W. R.; Krastev, R. Effect of Gas Type on Foam Film Permeability and Its Implications for Foam Flow in Porous Media. *Adv. Colloid Interface Sci.* **2011**, *168*, 71−78.
(37) Langevin, D. Aqueous Foams and Foam Films: Stability and Aging. *C. R. Phys.* **2014**, *15*, 260−269.
(38) Pasquet, M.; Galvani, N.; Requier, A.; Cohen-Addad, S.; Höhler, R.; Pitois, O.; Rio, E.; Salonen, A.; Langevin, D. Coarsening Transitions of Wet Liquid Foams under Microgravity Conditions. *Soft Matter* **2023**, *19*, 6833−6843.
(39) Matheson, I. B. C.; King, J. R. A. D. Solubility of Gases in Micellar Solutions. *J. Colloid Interface Sci.* **1978**, *66*, 464−469.
(40) Cramer, J. A.; Ananth, R. Permeability of a Thick Surfactant Film Enhanced by Micelles above Critical Permeation Concentration. *Colloids Surf., A* **2026**, *749*, 141395.
(41) Vakarelski, I. U.; Langley, K. R.; Yang, F.; Thoroddsen, S. T. Interferometry and simulation of the thin liquid film between a free-rising bubble and a glass substrate. *Langmuir* **2022**, *38*, 2363−2371.

Downloaded from pubs.acs.org/langd5/article-pdf/42/43/31793/6890141O/acs.langmuir.6c03871.pdf by guest on 08 November 2026

https://doi.org/10.1021/acs.langmuir.6c03871
Langmuir 2026, 42, 31793−31806